Stearic acid crystals stabilization in aqueous polymeric dispersions

Ahmed Jarray, Vincent Gerbaud, Mehrdji Hemati

Stearic acid crystals stabilization in aqueous polymeric dispersions

Ahmed Jarray[*], *Vincent Gerbaud*[1], *Mehrdji Hemati*

Université de Toulouse, INP, UPS, LGC (Laboratoire de Génie Chimique), 4 allée Emile Monso, F-31432 Toulouse Cedex 04, France

Keywords:
Agglomeration
Mesoscale simulation
Colloids
Coating
DPD

A B S T R A C T

In wet granulation processes, coatings or binders generally consist of mixtures of various raw materials that confer or enhance specific properties to the final product. Typically, a coating solution is composed of water, film forming polymer (such as hydroxypropylmethylcellulose, HPMC) and filler (such as stearic acid, SA).

One of the important issues in wet granulation processes is the stability of the aqueous coating (or binder) dispersion. An unstable dispersion results in the agglomeration of the colloidal particles, thereby affecting the film coating properties and eventually the coating process.

In this study, we use dissipative particle dynamics (DPD) to elucidate the structure of aqueous colloidal formulations. DPD is a coarse-grained molecular dynamics simulation method where the materials are described as a set of soft beads interacting according to the Flory–Huggins (1942) model. The DPD simulation results are compared to experimental results obtained by Cryogenic-SEM and particle size distribution analysis.

It is shown from the DPD simulation results that the HPMC polymer is able to form a layer that covers SA particles and thus produces stable colloids. Microcrystalline cellulose (MCC) also covers SA agglomerate but it is not able to diffuse inside its inner core. The agglomerate structure is characterized via the density distribution and the polymer chain end-to-end distance.

Experimental results show similar trends; particle size distribution analysis shows that in the presence of HPMC, the majority of SA particles are below 1 μm in diameter, also MCC is able to prevent the formation of big SA agglomerates and may be a better stabilizing agent than HPMC. SEM images reveal that HPMC surrounds SA agglomerates with a hatching textured film and anchors on their surface.

1. Introduction

Coating process involves the covering of particulate materials including seeds, agglomerates, pellets and powders with a surrounding layer of a coating agent (or coating material) (Salman et al., 2007). The macroscopic properties of the coated granule depend on the properties of the constituent phases of the coating agent, the coating-granule affinity interactions, and the texture of the coating and surface appearance (Salman et al., 2007). A coating material (or binder) should; (a) be suitable with the primary particles (or granule) onto which they it will be pulverized, (b) provide the quality requirements and the expected properties in the final products and (c) be compatible with the equipment used in the granulation process

* *Corresponding author*. Tel.: +33 0 6 48 45 57 31.
E-mail addresses: ahmed.jarray@ensiacet.fr, jarray42@gmail.com (A. Jarray), vincent.gerbaud@ensiacet.fr (V. Gerbaud), mehrdji.hemati@ensiacet.fr (M. Hemati).
[1] Tel.: +33 0 5 34 32 36 51.
http://dx.doi.org/10.1016/j.cherd.2016.02.028

Nomenclature

a_{ij}	interaction parameter between bead i and bead j
Cr	the harmonic spring constant
C_n	characteristic ratio of the polymer
Cv	width of the particle size distribution
d	particle diameter
f_i	sum of the forces acting on the bead i
F^C	conservative repulsive force
F^D	dissipative force
F^R	random force
F^S	bonding spring force
k_B	Boltzmann constant
l_i	distance between two attached beads
M_w	molecular weight of the polymer
M_m	molecular weight of the monomer
n_{DPD}	DPD number
N_m	coarse-grain number
$\vec{r}$	end-to-end distance vector
r_c	cutoff radius
r_i	position of the bead i
T	temperature
V_i	volume of the bead i
v_i	velocity of the bead i
ρ	number density
e	density
δ	solubility parameter
ξ_{ij}	random parameter
∂	parameter of dissipation
θ	adjustment parameter
χ_{ij}	Flory–Huggins parameter
ω	weight function
–	upper-script that denotes the property in DPD units

(e.g., sprayable by the designed turbine). Therefore, formulating the right coating solution (or binder) is important.

The coating solution or the binder is usually prepared through aqueous polymer dispersion. Hydrophilic stabilizing polymers (such as hydroxypropyl-methylcellulose, HPMC) and hydrophobic filler (such as stearic acid, SA) are added during the preparation of the polymer dispersion. These compounds will be present in the final binder or coating, therefore, they will affect various properties of the final product. The film forming dispersions should be physically stable and the particles should be uniformly dispersed in the medium, otherwise, uncompleted film formation may occur. For aqueous coating formulation to be successful, stable colloidal suspensions should be obtained.

In this context, considering that the agglomerate materials we are studying are composed of many molecules and have a size between 0.1 and 100 μm, it is relevant to perform mesoscale simulations, where molecules are represented as polyatomic beads. Interactions at the mesoscopic scale can be evaluated by the method called "dissipative particle dynamics" (DPD), this method generates a force field that gives a description of the dynamic behavior of the molecules that make up the polymer by reducing the degrees of freedom of the atoms, hence, making the simulation much faster. Groot and Warren (1997) have shown that the Flory–Huggins parameter χ can be used to assess the repulsive interactions in the DPD theory.

In this work, we investigate the structure of aqueous colloidal formulations at the mesoscale level with molecular simulations and experiments. This study is organized as follows: first, we will give a theoretical overview of the DPD method and the coarse-grain modeling. Then, we present the DPD model that we have developed to predict the behavior of polymer such as HPMC and microcrystalline cellulose (MCC) in the presence of hydrophobic filler (SA) in aqueous systems. This is followed by an experimental study of the formulation structures using Cryogenic-SEM and laser diffraction particle size analyser.

2. Background

2.1. *The DPD method*

The dissipative particle dynamics method (DPD) is a particle mesoscopic simulation method based on the formalism of Langevin (1908) with conservation of the momentum. The DPD method can be used for the simulation of systems involving colloidal suspensions, emulsions, polymer solutions, Newtonian fluids and polymer melts. This method enables accessing larger spatio-temporal scales than those in the molecular dynamics.

Recently, a number of workers have used the DPD method to study several phenomena. Groot (2003) used the DPD method to study the aggregation of surfactant. Rekvig et al. (2004) adopted the DPD method for the simulation of interacting oil–water–surfactant interfaces. The DPD method was also used by Hoogerbrugge and Koelman (1992) and by Boek et al. (1996, 1997) for the simulation of colloidal suspensions. Novik and Coveney (1997, 1998) used this method to study phase separation in binary immiscible fluids. To run simulations of polymer systems, Schlijper et al. (1995), Schulz et al. (2004, 2005), Tomasini and Tomassone (2012), and Cao et al. (2005) also used DPD simulations. Gama Goicochea (2007) used it to study polymer adsorption. Mayoral and Nahmad-Achar (2012) studied the interfacial tension between an organic solvent and aqueous electrolyte solutions and found good agreement with experimental data. The DPD method has also been used for the simulation of number of other physical systems and material interactions which are not considered in this study, including the behavior of lipid bilayer membranes (Venturoli and Smit, 1999), nanoparticles in brush polymer (Guskova et al., 2009) and flow in pores (Liu et al., 2007).

2.2. *Materials description: HPMC, MCC and SA*

Stearic acid is a fatty acid, and a hard, white or faintly yellow-colored, somewhat glossy, crystalline solid or a white or yellowish white powder (Rowe et al., 2009), and practically insoluble in water (Yalkowsky and He, 2003). Stearic acid is widely used in oral and pharmaceutical formulations as a tablet and capsule lubricant (Iranloye and Parrott, 1978; Mitrevej and Augsburger, 1982).

Hydroxypropyl-methylcellulose or Hypromellose (HPMC) is an odorless and tasteless, white or creamy-white fibrous or granular powder (Rowe et al., 2009). It is soluble in cold water, forming a viscous colloidal solution; practically insoluble in hot water. HPMC is used as a protective colloid by coating hydrophobic particles with multimolecular layer and promote

wetting (Mahato and Narang, 2011). In oral products, HPMC is mainly used as a tablet binder (Chowhan, 1980), in film-coating as a film former and as a matrix for use in extended release tablet formulations (Rowe, 1977). In addition, HPMC is used as an emulsifier, suspending agent and stabilizing agent in topical gels and ointments.

Microcrystalline cellulose (MCC) is a purified cellulose, practically insoluble in water and most organic solvents, produced by converting fibrous-cellulose to a redispersible gel or agglomerate of crystalline cellulose using acid hydrolysis (Milani and Maleki, 2012). MCC Presents a high cohesion and poor flowing characteristics (Chitu, 2009). MCC is widely used in pharmaceuticals, primarily as a binder/diluent in oral tablet and capsule formulations (Enézian, 1972).

Stearic acid (SA) is often added to the cellulose derivatives to enhance specific properties. For example, adding SA to HPMC leads to a decrease in the water affinity due to SA hydrophobic properties caused by its content of long-chains (Jiménez et al., 2010). Several studies have focused on the influence of SA on HPMC polymer; Jarray et al. (2015) found that HPMC and SA do not interact in dry systems, which may results in friable agglomerate or incomplete coating film. However, when they are placed in water, HPMC surround SA particles. Laboulfie (2013) found that HPMC is a good stabilizer for SA crystals. Fahs et al. (2010) investigated the surface properties of HPMC films formulated with SA as additive and found that the hydrophobic character of SA leads to the decrease of adhesion and friction of the coating film. They also found that HPMC formulated films were strongly dependent on SA content. Lara-Hernández et al. (2009) found that the hydration volume, the tablet hardness and the ejection pressure decrease as the stearic acid content increases in the HPMC drug formulations. They also found that drug dissolution increases with increasing proportions of SA and decreasing proportions of the HPMC in the tablets. Hagenmaier and Shaw (1990) studied the moisture permeability and tensile strength of edible films made with stearic acid and HPMC and found that permeability increased in the absence of SA.

One of the important issues, when preparing coating solutions and binders containing HPMC and SA, is the stability of the SA colloidal particles since any colloidal particle agglomeration could negatively impact the performance of the final coating solution. For aqueous coating formulation to be successful, stable colloidal suspensions should be obtained.

2.3. *Colloidal behavior and stabilization*

A particle suspension (such as stearic acid) in a liquid medium (e.g., water) is called colloidal when the particles are large enough to present a structure and small enough to be submitted to Brownian motion. Their size range is typically between 10 nm and several microns.

A colloidal dispersion is said to be stable when the colloidal particles remains dispersed over a long time scale (i.e., the total number of particles remains constant over time). If the particles are instable in a suspension, agglomeration may occur and may lead to sedimentation or creaming, and finally phase separation (Fig. 1).

To stabilize the particles in dispersion, polymer may be added. The role of polymers in the stabilization process during coating solution preparation can be classified into two phases; (a) the initial dispersion of the particles in the medium (normally with shear) and (b) the stabilization of that dispersion (without shear) (Vincent, 1974). The protective action by an adsorbed polymer layer is now generally referred to as "steric stabilization", steric stabilization acts essentially by preventing the approach of the particle cores to a separation where their mutual van der Waals attraction would be sufficient for agglomeration to occur (Vincent, 1974).

Polymeric stabilization requires that the solid particle provides an adsorbing substrate for the polymer and that the polymer is irreversibly adsorbed (Gregory, 1978). Much emphasis has been placed on the thickness of the adsorbed layer that confers to the particles a barrier against agglomeration. In this context, Koelmans and Overbeek (1954) suggested that only if the thickness of the adsorbed layer was comparable in size to the diameter of the dispersed particles could a polymeric steric mechanism provide sufficient protection. Walbridge and Waters (1966) showed that the minimum polymer barrier thickness required for the largest particles was of the order of 5 nm. Finally, some recent experiments by Crowl and Malati (1966) indicated the importance of good anchoring of the polymer on the surface of the colloid particles in the stabilizing process.

3. DPD method equations and "coarse-grain" modeling

3.1. *The "coarse-grain" modeling*

The computation cost in molecular simulation is proportional to the size and number of molecules placed in the simulation cell. Therefore, in order to access the mesoscopic scale, one solution is to convert the molecules (or segments of polymer chains) into representative entities which include only the molecular details essential to describe the system in the mesoscopic scale. These entities are called "beads". The conversion of molecules into beads is done through the "coarse-grain" approach which can reduce the degree of freedom of a molecule, thus, reducing the computational complexity of the system. Following this approach, a polymer chain is represented by a set of beads connected together by a harmonic spring.

Simulations in the DPD system are performed in reduced units. The reduced number density $\bar{\rho}$ in the DPD system is related to the real number density ρ of the compound by the following relationship:

$$\bar{\rho} = \rho r_c^3 \tag{1}$$

where, $\bar{\rho}$ is the number of beads in one cubic simulation cell of volume r_c^3, the cut-off radius r_c represents the unit length in the DPD system and is also used to establish the reference scale. Through this paper, the upper-script "–" denotes the property in the DPD system.

The coarse-graining degree N_m represents the number of molecules of water placed in a single bead. Grouping several molecules of water in one bead is used to match the volume of the different beads in the DPD simulations. N_m can be evaluated using the following formula:

$$N_m = \frac{\bar{\rho}_{molecule}}{\bar{\rho}} \tag{2}$$

where, $\bar{\rho}_{molecule}$ is the number of molecules in one cubic unit cell of volume r_c^3.

The coarse-grain parameter N_m is used to establish the reference scale. The cut-off radius r_c, representing the unit length

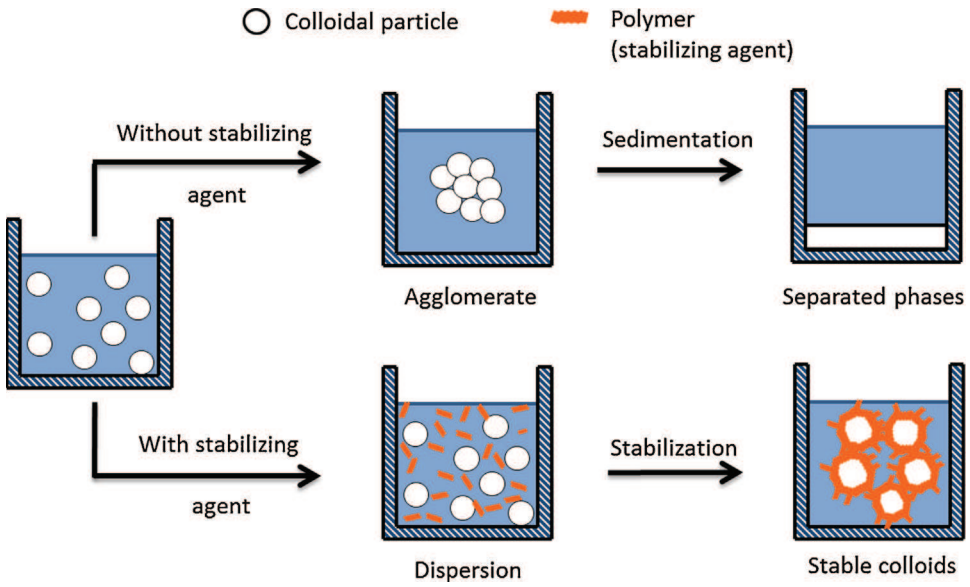

Fig. 1 – Schematic presentation of colloidal stability, with and without stabilizing agent.

in the DPD system can be obtained by using the following relationship:

$$r_c = 3.1072(N_m\tilde{\rho})^{1/3}\,\text{in Å} \tag{3}$$

3.2. *The DPD method equations*

In the DPD method, the compounds are composed of molecules described as a set of soft beads that interact dynamically in a continuous space and move along the Newton momentum equation. These interactions between the soft beads govern the affinity between the compounds and therefore control the final structure built by the beads in the DPD simulation. The total force f_i acting on the beads in the DPD simulation is given by the following expression:

$$f_i = \sum_{j\neq i}(F_{ij}^C + F_{ij}^D + F_{ij}^R + F_{ij}^S) \tag{4}$$

F_{ij} represent the force exerted by a bead i on the bead j. Each bead is subjected to three non-bonding forces; conservative repulsive force F^C that determines the thermodynamic behavior of the system, a dissipative force F^D which includes the friction forces and a random term F^R accounting for the omitted degrees of freedom (Español et al., 1997), and a bonding force F^S. These forces are trained by neighboring beads and delimited by the cut-off radius r_c.

$$\begin{aligned} F_{ij}^C &= a_{ij}\omega(r_{ij})\hat{r}_{ij} \\ F_{ij}^D &= -\partial\omega^2(r_{ij})(\hat{r}_{ij}\vec{v}_{ij})\hat{r}_{ij} \\ F_{ij}^R &= \sigma(\Delta t)^{-1/2}\omega(r_{ij})\xi_{ij}\hat{r}_{ij} \end{aligned} \tag{5}$$

where, $\vec{r}_{ij} = r_i - r_j$, $r_{ij} = |\vec{r}_{ij}|$, $v_{ij} = v_i - v_j$, $\hat{r}_{ij} = \vec{r}_{ij}/r_{ij}$ and $a_{ij} = a_{ji}$.

This last term a_{ij} represents the maximum repulsion between two beads; it encompasses all the physical information of the system. ∂ is the parameter of dissipation and ξ_{ij} is a random parameter which describe the noise with a zero mean and one unit variance. $\omega(r_{ij})$ is a weight function which determines the radial dependence of the repulsive force:

$$\omega(r_{ij}) = \begin{cases} 1 - r_{ij}/r_c, & \text{if } r_{ij} \le r_c \\ 0, & \text{if } r_{ij} \ge r_c \end{cases} \tag{6}$$

Non-bonded forces act within a sphere of radius r_c. Outside this sphere, interaction forces are ignored. More details about the DPD method are given by Trofimov (2003).

The connected beads in a polymer chain undergo spring bond strength:

$$F_{ij}^S = Cr\, r_{ij} \tag{7}$$

According to the literature, the harmonic spring constant Cr gives good results for values between 2 and 4 DPD (i.e., between 75 and 150 $J\,mol^{-1}\,Å^{-2}$) (Groot and Warren, 1997), which is sufficient to maintain the adjacent beads well-connected in the polymer chain.

An important parameter in the DPD method is the term a_{ij} of the conservative force, which represents the maximum repulsion between two unlike beads; it encompasses all the physical information of the system. It can be determined according to a linear relationship with the Flory–Huggins parameter χ_{ij}:

$$\tilde{a}_{ij}(\tilde{\rho} = 3) = \tilde{a}_{ii} + \frac{\chi_{ij}}{0.286} \tag{8}$$

The number density $\tilde{\rho}$ is equal to 3 DPD units, for which the repulsion parameter/Flory–Huggins parameter relationship has been defined (Groot and Warren, 1997).

The Flory–Huggins values can be calculated from the Hildebrand solubility parameter (Hildebrand, 1950) using the formula:

$$\chi_{ij} = \frac{(\delta_i - \delta_j)^2(V_i + V_j)}{2k_BT} \tag{9}$$

where, V is the volume of the beads, δ_j and δ_i are the solubility parameters of beads i and j respectively.

To relate the DPD soft sphere model to a realistic thermodynamic state, Groot and Warren (1997) obtained the following

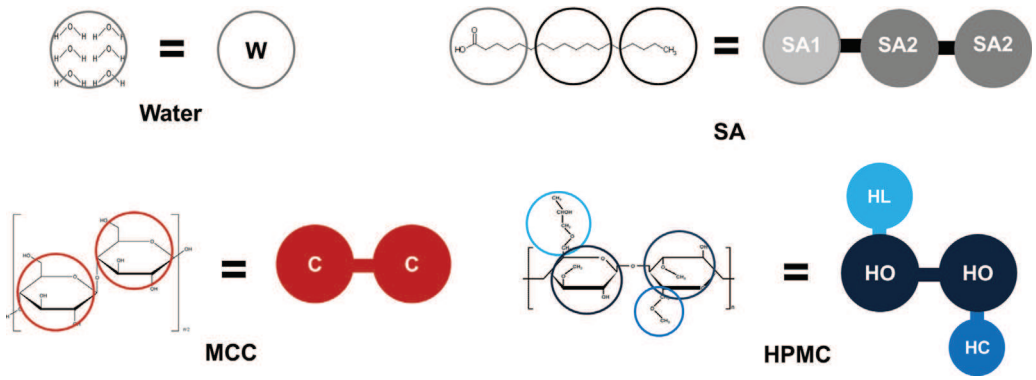

Fig. 2 – "Coarse-grain" method; molecules and monomer conversion into beads for water (W), stearic acid (SA), microcrystalline cellulose (MCC) and hydroxypropyl-methylcellulose (HPMC).

expression of the repulsion parameter a_{ii} between the same beads:

$$\bar{a}_{ii} = \frac{(16N_m - 1)}{2\theta\bar{\rho}} \tag{10}$$

where, θ is an adjustment parameter equal to 0.101 ($\pm$0.001).

For polymers, the number of beads that composes one polymer chain can be estimated with the number of DPD n_{DPD}:

$$n_{DPD} = \frac{M_w}{M_m C_n} \tag{11}$$

M_w is the molecular weight of the polymer, M_m the molecular weight of the monomer and C_n the characteristic ratio of the polymer.

3.3. *"Coarse-grain" model and DPD parameters*

All atom molecular simulation was performed first to calculate the solubility parameter of HPMC, MCC, SA and water. Then, for the purposes of DPD simulations, the molecular structure of each compound was subjected to a coarse grain mapping, thus, transformed into a mesoscopic model constituted of beads. The repulsive interactions between the beads are obtained using Eqs. (8) and (10) where the solubility parameter is used as input.

3.3.1. *The mesoscale "Coarse-grain" model*

The task of finding the adequate coarse-grain model comprises two concomitant parts: estimating the most suited volume of the bead and avoiding the solidification of the system. In this context, we select the reference volume of a single bead equal to 180 Å^3, because, as we will see later, it allows assimilating each molecule or monomer to a bead whose volume is close to that value. Thus, a water bead must represent 6 water molecules (volume of a water molecule $\approx$30 Å^3), which roughly corresponds to a single monomer of MCC. SA is thus composed of 3 beads; one bead containing the fragment SA1 and two beads of the fragments SA2. HPMC repeating unit is coarse-grained into 4 beads (one HL, two HO and one HC (see Fig. 2)). This way, all the beads have approximately the same volume.

Since number density $\bar{\rho}$ is equal to 3, a cubic simulation cell with an edge length equal to r_c contains three beads with 6 molecules of water each and corresponds to a volume of 540 Å^3. The chemical structure of our materials and their conversion into beads are shown schematically in Fig. 2.

3.3.2. *Molecular dynamic simulation and solubility parameter calculation*

Following our previous work (Jarray et al., 2015), the solubility parameters needed to compute the Flory–Huggins parameter χ are calculated using either molecular simulations (in Biovia's Material Studio software product (Biovia, 2013)) or Yamamoto's molecular breaking method (HSPiP, 2010) and are presented in Table 1. Molecular simulations were performed with an integration step of 1 femtosecond (fs). The interatomic interactions are described by the COMPASSII (Condensed-phase Optimized Molecular Potentials for Atomistic Simulation Studies) force field (Sun, 1998) along with Ewald summation. NPT dynamics (constant temperature and pressure) was performed first to equilibrate the density of the system for 500 picoseconds (ps) at room temperature (T = 298 K) and atmospheric pressure (P = 1 atm), then, we ran the simulation in the canonical dynamics ensemble NVT (constant temperature and density) at a temperature T = 298 K for 500 ps in order to track the convergence of the cohesive energy density. The last 50 ps were used for averaging potential energy components. Hildebrand solubility parameters for each repeating unit and molecules were calculated as well as their standard deviations (see Table 1). Results obtained by molecular simulation are used next as input parameters in the DPD simulations.

In Table 1, results obtained by molecular simulation are close to HSPiP predictions. Molecular simulation results will be used next as input parameters in the DPD simulations. Table 2 shows the beads volume calculated by dividing the molecular weight M_w by the density e. As anticipated, the beads volume and radius are close. Thus, our choice of a reference volume equal to 180 Å^3 is good.

3.3.3. *DPD simulation parameters*

The individual self-repulsive interaction parameters a_{ii} were determined using Eq. (10). It is equal to 157 when N_m = 6. The conservative force parameters a_{ij} between every couple of beads were then calculated using Eq. (8). The results are summarized in Table 3. The number of beads used to describe the HPMC polymer in the DPD simulations is determined by the DPD number n_{DPD} which was calculated using Eq. (11). The ratio characteristic was computed using Material Studio's (Biovia, 2013) Synthia module (Bicerano, 2002). We found that the HPMC polymer chain is composed of 10 repetitions (n_{DPD} = 10), and the MCC polymer is composed of 44 beads (n_{DPD} = 44).

All DPD simulations were performed by the Materials Studio 7 software (Biovia, 2013). A $30 \times 30 \times 30$ r_c^3

Table 1 – Solubility parameter and density of repeating units and molecules.

Compounds	Solubility parameter δ of the repeating unit and molecule $(J\,cm^{-3})^{1/2}$		Density e of the repeating unit and molecule $(g\,cm^{-3})$	
	COMPASSII	HSPiP	COMPASSII	HSPiP
HPMC				
HL	22.1 ± 0.6	22.4	0.893 ± 0.02	0.918
HO(×2)	27.3 ± 0.3	25.5	1.233 ± 0.01	1.204
HC	18.0 ± 0.5	17.5	0.768 ± 0.02	0.700
SA				
SA1	23.4 ± 0.3	20.4	0.963 ± 0.01	0.924
SA2(×2)	14.5 ± 0.2	15.0	0.648 ± 0.01	0.676
MCC	31.5 ± 0.6	32.0	1.347 ± 0.02	1.434
Water	47.5 ± 0.4	47.8[a]	0.962 ± 0.01	0.997[a]

HPMC: hydroxypropyl-methylcellulose, SA: stearic acid, MCC: microcrystalline cellulose.
[a] HSPiP (2010) Yamamoto database.

Table 2 – Conversion of monomer and molecules into beads, and properties of the beads.

Compounds	M_w of the repeating unit and molecule $(g\,mol^{-1})$	Bead volume (Å^3)		Bead radius (Å)	
		COMPASSII	HSPiP	COMPASSII	HSPiP
HPMC					
HL	89.1	165.7	161.2	3.41	3.37
HO (×2)	144.2	194.2	198.8	3.59	3.62
HC	45.1	97.5	106.9	2.85	2.95
SA					
SA1	115.2	198.6	207.1	3.61	3.67
SA2 (×2)	85.2	218.3	209.3	3.73	3.68
MCC	162.2	199.9	187.8	3.62	3.55
Water	18.0	186.4	179.9[a]	3.54	3.50

HPMC: hydroxypropyl-methylcellulose, SA: stearic acid, MCC: microcrystalline cellulose.
[a] HSPiP (2010) Yamamoto database.

Table 3 – The conservative force parameter a_{ij} between the beads.

a_{ij}	HL	HO	HC	SA1	SA2	MCC	Water
HPMC	HL	157.00					
	HO	161.12	157.00				
	HC	158.82	167.56	157.00			
SA	SA1	157.26	159.54	160.58	157.00		
	SA2	166.33	185.51	158.66	170.89	157.00	
MCC	170.50	159.85	179.56	167.92	207.65	157.00	
Water	252.37	222.05	260.48	250.89	342.12	198.64	157.00

HPMC: hydroxypropyl-methylcellulose, SA: stearic acid, MCC: microcrystalline cellulose.

(i.e., $24.4 \times 24.4 \times 24.4\,nm^3$) simulation cell box was adopted where periodic boundary conditions were applied in all three directions. According to Eq. (3), the cut-off radius $r_c = 8.314$ Å. The dissipation parameter $\gamma = 4.5$ DPD units (i.e., $0.09043\,g\,mol^{-1}\,fs^{-1}$) which is the recommended value proposed by Groot and Warren (1997) to ensure a stable simulation and a physically meaningful system. Each DPD simulation runs 1000 DPD units (i.e., 5374.17 ps) which is sufficient to get a steady phase. The time step increases proportionally with the CG number N_m (Groot and Rabone, 2001), hence, it is preferable to reduce the integration time, we took $t = 0.02$ units DPD (i.e., 107.483 fs) rather than 0.04 DPD units adopted by Groot and Warren (1997). DPD simulations work only in the canonical thermodynamic *NVT* ensemble, and the simulation were done at a temperature of $T = 298$ K. Initially the beads were randomly dispersed in the simulation cell. The DPD parameters are presented in Table 4.

4. Materials and experimental methods

4.1. *Materials*

The compounds chosen in this study are: hydroxypropyl-methylcellulose (HPMC) (H8384 Sigma), purified stearic acid (SA), microcrystalline cellulose (MCC, Avicel PH-101) and water. HPMC, SA and MCC were purchased from Sigma–Aldrich.

4.2. *Experimental methods*

4.2.1. *Cryogenic-SEM instruments*

Cryogenic-SEM is a technique that allows visual checking of the structure of dispersions (separated or agglomerated particles) in two dimensions by freezing the sample by ultra-rapid freezing not allowing time for ice crystals to grow. After

Table 4 – List of parameters used in DPD simulation.

Coarse grain number (N_m)	6
Simulation box size	$24.4 \times 24.4 \times 24.4\,nm^3$
Cut-off radius (r_c)	8.314 Å
Dissipation parameter (γ)	4.5 DPD units (i.e., 0.09043 g mol^{-1} fs^{-1})
DPD simulation time	1000 DPD units (i.e., 5374.17 ps)
Integration time	0.02 DPD units (i.e., 107.483 fs)
Temperature (T)	298 K

fracturing the sample, sublimation of the surface takes place in order to expose the first layer of particles inside the dispersion. Then, a beam scans the sample surface and in response retransmits particles. The fractured sample is then observed in a scanning electron microscope (Hitachi MEB ESEM Quanta 250 FEG FEI) of which the sample holder itself is cooled by liquid nitrogen. Various detectors are used to analyze these particles and to reconstruct an image of the surface. This technique is widely used by biologists or chemists (Glicksman, 2000) and in the food industry (Moor and Riehle, 1968).

4.2.2. *Particle size analyzer*

Most of the materials used in this study are stearic acid (SA) suspensions dispersed in a polymeric solution. The properties of dispersed material are strongly related to their particle size. Measuring of the particle size distribution was done using laser particle size analyzer MALVERN Mastersizer 2000. This instrument is equipped with a wet dispersion module type HYDRO that allows the characterization of particle size between 0.1 and 1000 μm. The particle size analyses reported throughout this study are the average of three successive laser diffraction runs.

4.3. *Preparation protocol of the HPMC-SA suspension*

HPMC-SA mixture was prepared by adding the cellulose polymer in deionized water previously heated to 80 °C. The mixture was then homogenized by moderate agitation for 30–60 min using a rotor–stator homogenizer (Ultraturrax T25, Janke and Kunkel, Germany) at 85 °C. Stearic acid was then added to the HPMC solution progressively under agitation until it was evenly dispersed. The mixture was then cooled using an ice bath under agitation for 30 min. Solutions were thereafter degassed at 50 mbar for 2 h. The readily prepared solutions were stored immediately at 5 °C for at least 24 h.

The same protocol was used for the preparation of MCC-SA mixtures.

5. Results and discussions

5.1. *DPD simulation results*

When preparing a coating solution, the challenge is to fabricate a polymeric coating solution with high hydrophobic SA content while maintaining the stability of the suspension. To this end, we used our DPD model to perform simulations of the coarse-grained HPMC-SA and MCC-SA structure in water.

An important requirement to prevent agglomeration is that the stabilizing agent has to be adsorbed strongly enough on the surface of the particle. If a polymer is only weakly adsorbed, then, it is possible that desorption can take place even during Brownian collisions (without deliberately shearing the system). Thus, agglomeration may take place within the system on standing (Vincent, 1974). Spontaneous, weak and slow agglomeration can also occur in systems where the adsorption is strong, but where the adsorbed layer is thin (Vincent, 1974). The strength of the adsorption in our DPD simulations can be assessed by the amount of stabilizing agent beads which are inside the agglomerate.

Fig. 3(a) shows a snapshot of configuration of HPMC–SA (10%–10% (w/w)) in water (transparent) at equilibrium state. Hydrophobic SA molecules agglomerate under the action of the repulsion forces of the water beads. At the same time, HPMC beads redistribute on the outer surface of the SA agglomerate. HPMC matrix completely surrounds SA through polymer entanglement and forms a thick layer between SA and water, preventing SA particles from escaping which correspond to the result obtained by Jarray et al. (2015) affinity model.

We also notice that a part of the HPMC polymer chain diffuses inside the SA inner core and strengthen the attachment between SA and HPMC, resulting in a stable SA microsphere, thus, confirming the experimental conclusions of Laboulfie (2013). Fig. 3(b) presents the concentration of the species throughout the simulation cell. A downward deviation in the water curve corresponds to an area that lacks water beads,

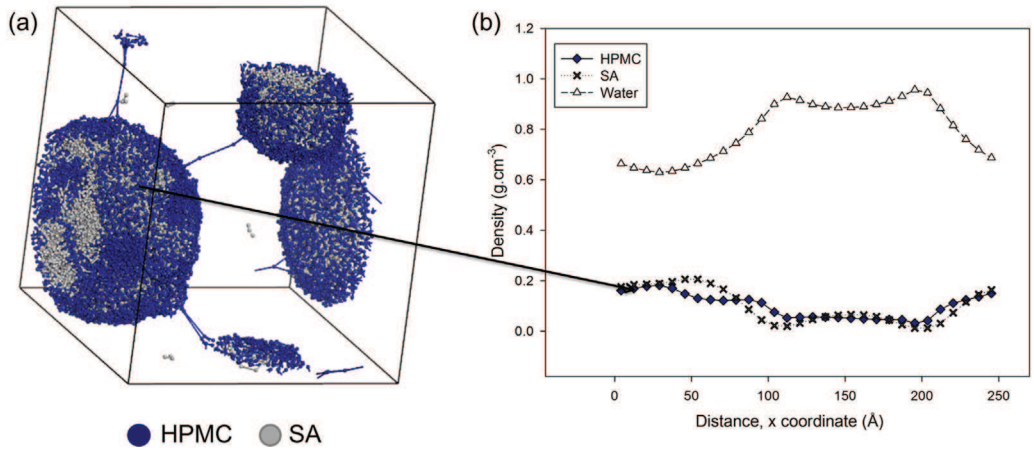

Fig. 3 – DPD simulation of HPMC (hydroxypropyl-methylcellulose, 10%(w/w))–SA (stearic acid, in light grey, 10% (w/w)) mixture in water (transparent, 80% (w/w)). (a) Snapshot of HPMC-SA-water simulation cell and (b) Density profile of HPMC, SA and water as a function of the *x* coordinate. (For interpretation of the references to color in this figure legend, the reader is referred to the web version of this article).

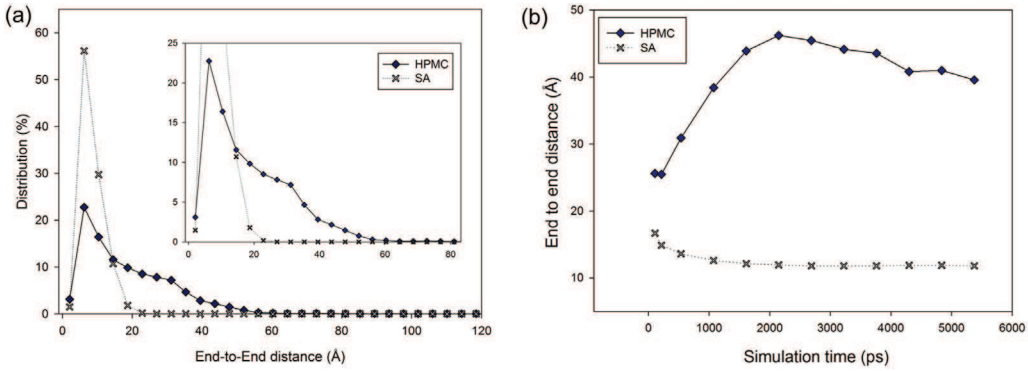

Fig. 4 – End-to-end distance of HPMC and SA in HPMC-SA mixture. (a) End-to-end distance of the last step of the DPD simulation and (b) RMS end-to-end distance as a function of time steps, each point is averaged over 10 successive steps.

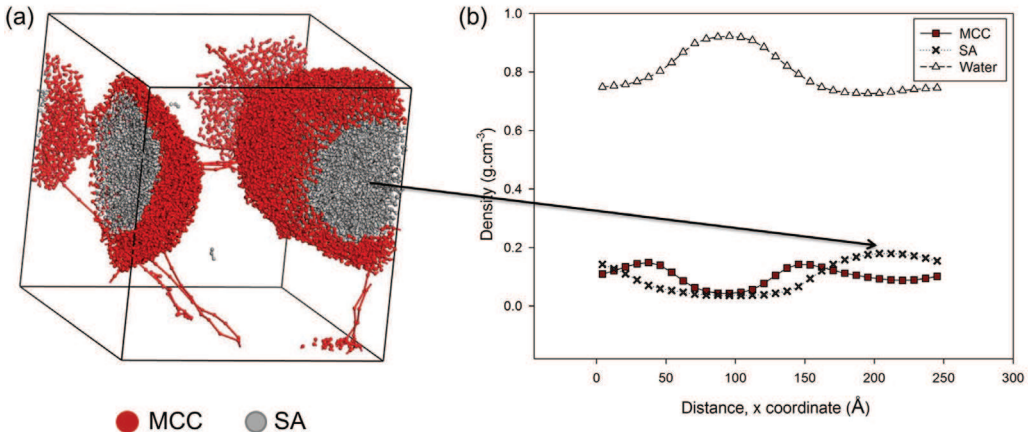

Fig. 5 – DPD simulation of MCC (microcrystalline cellulose, 10%(w/w))–SA (stearic acid, in light grey, 10% (w/w)) mixture in water (transparent, 80% (w/w)). (a) Snapshot of MCC-SA-water simulation cell and (b) Density profile of MCC, SA and water as a function of the *x* coordinate. (For interpretation of the references to color in this figure legend, the reader is referred to the web version of this article)

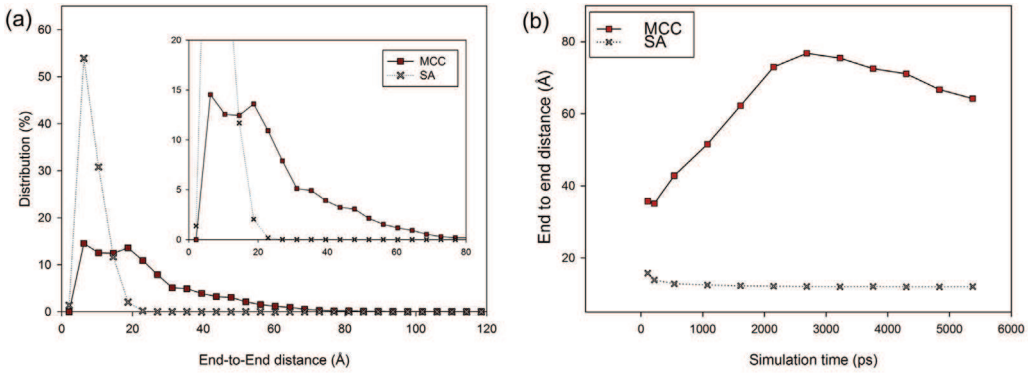

Fig. 6 – End-to-end distance of MCC and SA in MCC–SA mixture. (a) End-to-end distance of the last step of the DPD simulation and (b) RMS end-to-end distance as a function of time steps, each point is averaged over 10 successive steps.

in the same way, upward deviation in the SA curve translates into bigger agglomerate.

In Fig. 4(a), we present the end-to-end distance $\vec{r}$ distribution curve of HPMC polymer at the last simulation step, and we compare it to the end-to-end distance of SA. This parameter is the distance between one end of a polymer chain (or long molecule) to the other end, and thus describes the coiling degree of a polymer chain:

$$\vec{r} = \sum_{i}^{n_{DPD}} \vec{l}_i \tag{12}$$

where, l_i the distance between two attached beads in the same polymer, and n_{DPD} is the number of beads in the polymer. Because of their low chain length compared to HPMC, SA end-to-end distribution curve show a pronounced peak and a narrower curve than HPMC. The curves are spread between

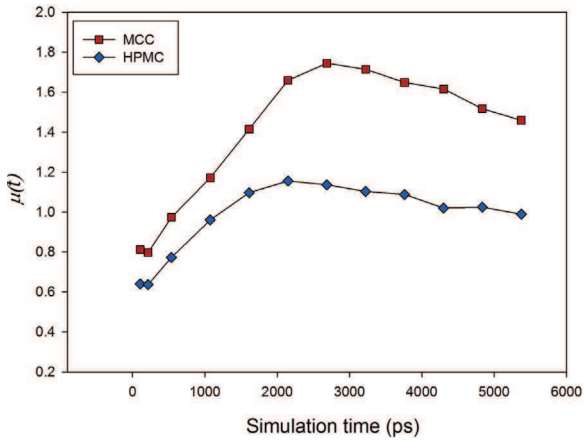

Fig. 7 – Average $\mu(t)$ as a function of time steps.

2 and 50 Å for HPMC and between 2 and 20 Å for SA. HPMC's maximum polymer length is between 35 and 45 Å. It appears that SA agglomerate forces the surrounding HPMC chains to straighten-up.

Fig. 4(b) shows the evolution of the average RMS end-to-end distance as a function of time steps (i.e., the root mean square of the length of the polymer):

$$\langle r^2 \rangle^{1/2} = \left(\sum_{i}^{n_{DPD}} \langle l_i^2 \rangle + 2 \sum_{i<j}^{n_{DPD}} \langle \vec{l}_i \times \vec{l}_j \rangle \right)^{1/2} \quad (13)$$

Each value of the RMS end-to-end distance is averaged over 10 simulation steps. We can see from Fig. 4(b) that, at the end of the simulation, the length of the RMS end to end distance of HPMC polymer is around 40 Å, and roughly equal to 15 Å for SA. This corresponds to the highest end-to-end distance of HPMC and SA observed in Fig. 4(a). We notice also that the RMS end-to-end distance of SA decreases until the simulation time is 1000 ps, and then remains constant. This means that SA is aggregating and the distance between the joined beads of SA molecules decreases under the action of the strong repulsive forces of the water beads and HPMC beads. On the other hand, HPMC's RMS end-to-end distance starts increasing rapidly until the 2200th time unit. This is the time before which the spherical SA agglomerate was formed and the HPMC polymer starts covering the formed agglomerate. The small decrease in the RMS end-to-end distance of HPMC polymer chains at the end of simulation is due to the compression and stretching of the spherical agglomerate before reaching the equilibrium state.

Fig. 5(a)shows the final structure of MCC–SA (10%–10% (w/w)) in water (transparent) when equilibrium state is reached. In Fig. 5(b), we present the concentration of the materials throughout the simulation cell along the *x*-coordinate. MCC completely surrounds SA agglomerate and interposes on its surface without diffusing inside its core and forms a spherical shape. Comparing to HPMC-SA case, the density distribution of MCC and SA along the *x* coordinate is more dissimilar, indicating less MCC beads that diffuse inside SA agglomerate. Consequently, since colloidal dispersions always show Brownian motion and hence collide with each other frequently (Napper, 1983), the physical bond between SA and MCC is susceptible to detach, and SA particles could escape the MCC layer, and therefore, form large agglomerate.

MCC's end-to-end distance curve shown in Fig. 6(a) presents a wide distribution between 2 and 70 Å, the majority of the MCC chains have an end-to-end distance between 5 and 30 Å. The high end-to-end distance of MCC chains can be explained by the absence of MCC beads inside the SA agglomerate, because the less polymer beads that diffuse inside the SA agglomerate, the less coiled the polymer chains (i.e., since the beads do not diffuse inside the SA agglomerate, most of the MCC chains extend themselves to surround the SA agglomerate). In addition, MCC presents wider distribution than HPMC, indicating less coiled chains. This also can be confirmed by dividing the RMS end-to-end distance of HPMC and MCC by the number of beads in each polymer chain. Fig. 7 presents $\mu(t)$, which is equal to the RMS end-to-end distance divided by the number of beads, as a function of time simulation. $\mu(t)$ gives the coiling degree of polymer and it is not affected by the chain length. We can see that MCC has a higher $\mu(t)$ value, which indicates lower coiled chains of MCC compared to HPMC.

5.2. *Experimental results*

Fig. 8 shows photographs of the appearances of the samples used in this study. Pure SA in water shows phase separation (Fig. 8(a)) due to SA agglomeration. HPMC is soluble in water and forms a homogenous transparent solution (Fig. 8(b)). Pure

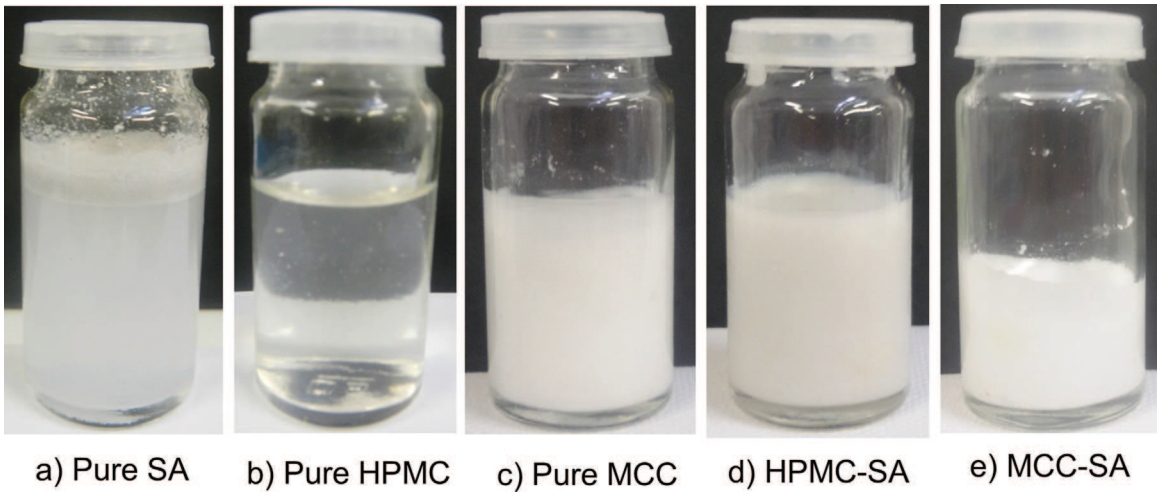

Fig. 8 – Appearances of (a) pure SA 10% (w/w), (b) pure HPMC 10% (w/w) and (c) pure MCC 10% (w/w), HPMC–SA 10%–10% (w/w), MCC–SA 10%–10% (w/w).

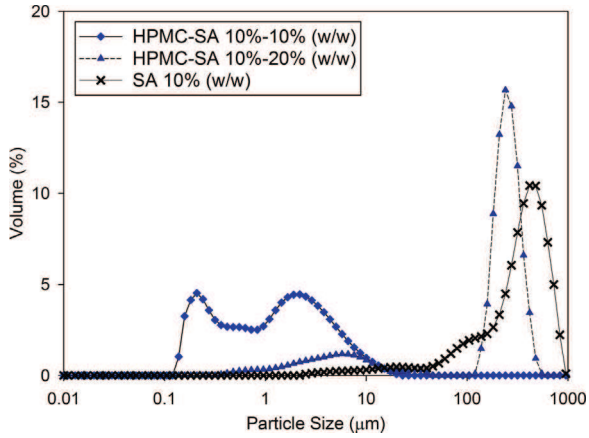

Fig. 9 – Particle size distribution in volume (%) for HPMC–SA (10%–10% (w/w)) in water and SA (10% (w/w)) in water, HPMC: hydroxypropyl-methylcellulose, SA: stearic acid.

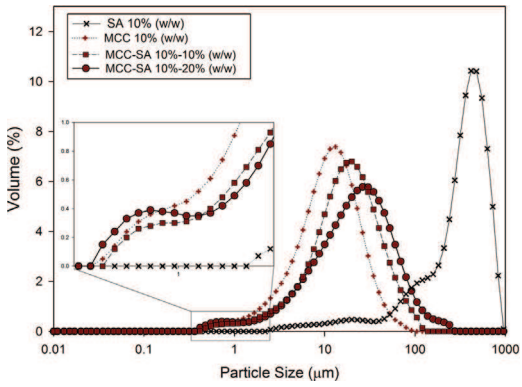

Fig. 10 – Particle size distribution of MCC–SA in water and SA (10% (w/w)) in water, MCC: microcrystalline cellulose, SA: stearic acid.

MCC in water forms a white solution (Fig. 8(c)). When mixing SA and HPMC in water, following the preparation protocol described above, a white homogenous solution is obtained and no phase separation can be observed by the naked eye (Fig. 8(d)). The same conclusions are obtained when mixing SA with MCC (Fig. 8(e)).

5.2.1. *Particle size distribution*

Prepared samples were subjected to laser diffraction particle size analyzer with a Master Sizer (MALVERN). The results in Fig. 9 are the average of three successive laser diffraction runs.

Particles size distribution of pure SA (10% in water), HPMC–SA (10%–10% (w/w) in water) and HPMC–SA (10%–20% (w/w) in water) are shown in Fig. 9. Table 5 shows the granular properties of each suspension, d_{10} and d_{90} are the particle sizes below which 10% and 90% of the particles respectively belong, and d_{32} is the surface weighted mean. The coefficient Cv in Table 5 measure the width of the distribution. The narrower the distribution, the lower the Cv value.

In pure SA (10% (w/w)) curve in Fig. 9, the majority of SA agglomerate have a size above 5 μm with a mean diameter of $d_{50} = 387.269$ μm. SA is insoluble in water and its hydrophobic character favors the agglomeration of SA molecules, thus, forming large cluster. Regarding HPMC–SA 10%–10% (w/w) mixture, the mean diameter is $d_{50} = 1.369$ μm. This means that most of the SA crystals are stabilized by the HPMC polymer with formation of some small agglomerate with a size between 1 and 15 μm. According to our DPD simulations, this is attributed to the covering of SA agglomerate by HPMC, and to the diffusion of HPMC beads inside it. At 20% of SA in HPMC–SA 10%–20% (w/w), the median particle size in volume increases significantly from 1.37 μm to 246.65 μm, and the size distribution curve shifts to higher distribution sizes and becomes narrower ($Cv = 1.47$). At this point, any other addition of SA particles will not have a noticeable effect on the stabilization of SA by HPMC.

Particles size distribution of aqueous solution of pure SA (10% (w/w)), pure MCC 10% (w/w), MCC–SA (10%–10% (w/w)) and MCC–SA (10%–20% (w/w)) are shown in Fig. 10. Pure MCC has a wide particle size distribution (Fig. 10) and a median particle size $d_{50} = 12.10$ μm. This is because MCC has a very low solubility in water. After adding 10% (w/w) of SA to MCC, the curve shifts a little to higher values of particle sizes and the median particle size is equal to 18.73 μm, which is notably lower than that of pure SA 10% (w/w). This indicates that MCC may be able to stabilize SA, but it's not as good as HPMC.

At 20% (w/w) of SA, we notice that MCC-SA particle distribution curve shifts slightly to higher values with a median size equal to 23.53 μm, but still, its particle size range is below that of HPMC–SA 10%–20% (w/w) (see Fig. 9), indicating that, for high values of SA (above 10%), MCC can prevent the agglomeration of SA particles. This also suggests that, for high percentages of SA, MCC is a better stabilizing agent than HPMC. Also, we notice that, at lower particles sizes range (below 1 μm), MCC–SA 10%–20% (w/w) has a higher particle distribution curve than MCC–SA 10%–10% (w/w) and MCC 10% (w/w) (Fig. 10), indicating an increase of the number of small particles at high SA contents. We infer that this is due to the small particles of SA; smaller than the MCC particles, which surround the big MCC particles.

5.2.2. *Cryogenic-SEM results*

To distinguish between HPMC and SA structure, two cryofixated samples were observed using transmission electron microscopy (SEM), the first sample contains 10% (w/w) of HPMC in water and the second one contains 10% (w/w) of SA in water.

From the overview SEM images in Fig. 11, we can distinguish between SA and HPMC. SA has the form of crystalline needles that form large agglomerate in water and their size is around 50 μm, while HPMC becomes amorphous and forms transparent solution which makes it difficult to distinguish between HPMC and water.

When the samples are sublimated (Fig. 11(b) and (d)), we notice that HPMC-water architecture shows a perforated structure designed by the sublimated ice crystals templates. The black background in Fig. 11(b) is the vitrified water. Cryofixation using pasty nitrogen is a slow freezing process that generates ice crystals inside the samples, consequently, inner parts of HPMC-water mixture freeze slower than the outer parts, and therefore, exhibit larger pores after sublimation.

SEM images in Fig. 12 agree with the particle size distribution results. Before sublimation (Fig. 12(a)), SA agglomerate is surrounded by a HPMC-water polymeric suspension. Most SA microcrystals have a size below 1 μm and some few others with a random shape have bigger size.

After sublimation (Fig. 12(b)), HPMC shows pores in the micrometer scale, patterned by the ice crystals. HPMC is well anchored on the surface of the SA agglomerate and covers it

Table 5 – Granular properties in volume of the dispersions.					
Sample	d_{10} (μm)	d_{50} (μm)	d_{90} (μm)	d_{32} (μm)	Cv
SA 10% (w/w)	81.32	387.27	684.62	105.93	1.56
HPMC–SA 10%–10% (w/w)	0.22	1.37	5.69	0.62	3.99
HPMC–SA 10%–20% (w/w)	5.14	246.65	369.45	13.70	1.47
MCC 10% (w/w)	3.524	12.10	29.65	6.89	2.16
MCC–SA 10%–10% (w/w)	5.08	18.73	50.91	9.54	2.45
MCC–SA 10%–20% (w/w)	4.96	23.53	71.53	9.24	2.83

HPMC: hydroxypropyl-methylcellulose, SA: stearic acid, MCC: microcrystalline cellulose.

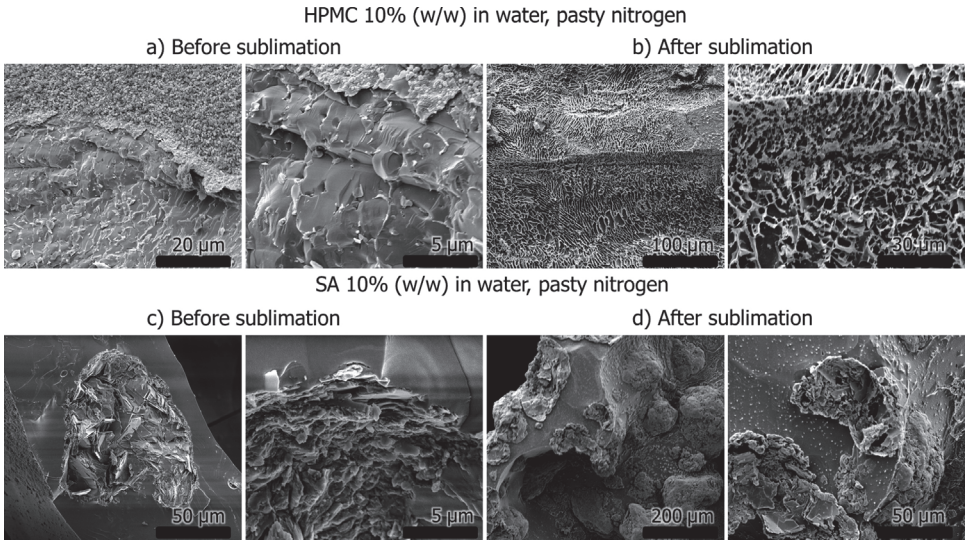

Fig. 11 – SEM micrographs of HPMC (top) and SA (bottom) in water before and after sublimation, cryofixated using pasty nitrogen. HPMC: hydroxypropyl-methylcellulose, SA: stearic acid.

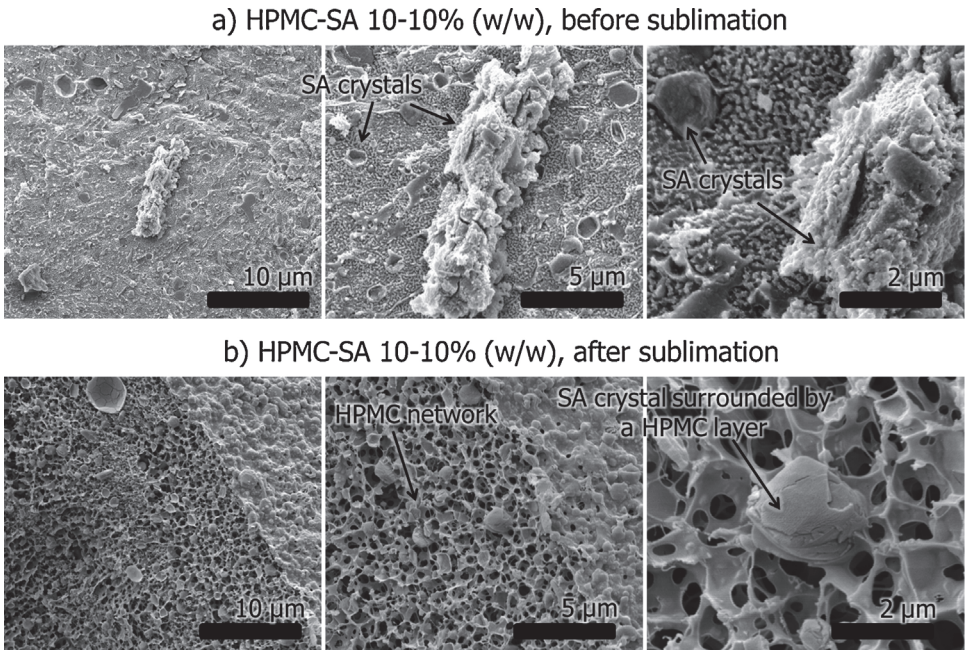

Fig. 12 – SEM micrographs of HPMC-SA in water and taken before and after sublimation. HPMC: hydroxypropyl-methylcellulose, SA: stearic acid.

with a hatching textured film that resembles dried soil. HPMC forms a gel network, immobilizing SA crystals and preventing their agglomeration.

Fig. 13 shows the SEM images of MCC–SA (10%–10%) mixture. After sublimation, we can see SA crystals with different sizes trapped in a network of MCC. This latter has a different structure than the matrix formed by HPMC polymer in the HPMC-SA case (Fig. 12(b)); it has different shapes; there are no perforations and the MCC network is like a crossing net. It seems also that MCC surrounds SA crystals without adsorbing in its surface since we can see the SA crystal needles in the SA agglomerate surface.

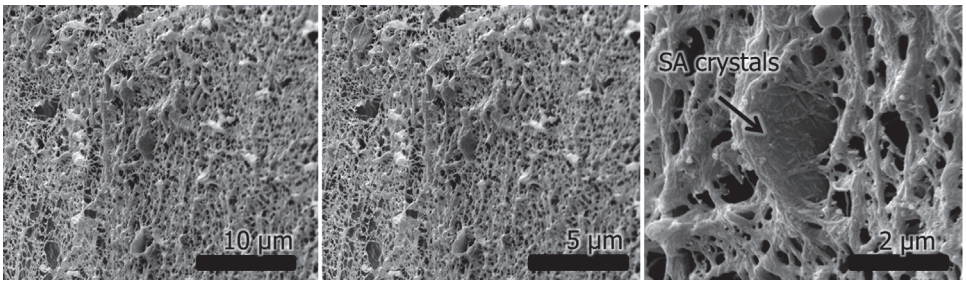

Fig. 13 – SEM micrographs of MCC–SA in water taken after sublimation. MCC: microcrystalline cellulose, SA: stearic acid.

6. Conclusion

In this study, we presented a mesoscale "coarse-grain" model for hydroxypropyl-methylcellulose (HPMC) microcrystalline cellulose (MCC) and stearic acid (SA). DPD method was applied to the "coarse-grain" model and dynamic simulation was launched, allowing to describe the structure of colloidal suspensions composed of the aforementioned compounds. DPD simulation results show that our "coarse-grain" model is able to reproduce some structural features of aqueous colloidal formulations.

According to DPD results, at a percentage of SA of 10% (w/w), HPMC completely covers SA agglomerates. Furthermore, a high amount of HPMC diffuses to the inner core of SA and reinforces the attachment with SA agglomerate, preventing further agglomeration. On the other hand, MCC surrounds SA agglomerate without diffusing inside it.

Experimental results show similar trends; HPMC-SA particle size distribution curve shows that the majority of SA particles are below 1 μm in size. Particle size distribution curves also showed that the small particles of SA surround the big particles of MCC. Furthermore, for high percentage of SA (above 10% (w/w)), MCC is able to prevent the formation of big SA agglomerates and, consequently, may be a better stabilizing agent than HPMC. By comparison with the DPD simulations results, the inability of MCC to diffuse inside the SA agglomerate, despite the complete coverage of SA by MCC, explains why MCC is unable to produce small SA particles, but able to prevent the formation of big SA agglomerates.

References

Bicerano, J., 2002. Prediction of Polymer Properties, 3rd ed. CRC Press, New York, pp. 784.

Biovia, Material Studio Suite release 7, 2013. ⟨http://accelrys.com/products/materials-studio/index.html.⟩.

Boek, E.S., Coveney, P.V., Lekkerkerker, H.N.W., 1996. Computer simulation of rheological phenomena in dense colloidal suspensions with dissipative particle dynamics. J. Phys: Condens. Matter 8 (47), 9509–9512.

Boek, E.S., Coveney, P.V., Lekkerkerker, H.N.W., van der Schoot, P., 1997. Simulating the rheology of dense colloidal suspensions using dissipative particle dynamics. Phys. Rev. E 55 (3), 3124–3133.

Cao, X., Xu, G., Li, Y., Zhang, Z., 2005. Aggregation of poly(ethylene oxide)-poly(propylene oxide) block copolymers in aqueous solution: DPD simulation study. J. Phys. Chem. A. 109 (45), 10418–10423.

Chitu, M.T.M., 2009. Granulation Humide Des Poudres Cohesives: Rheologie, Mecanismes de Croissance et Tenue Mécanique des Granules, Thèse de Doctorat. Université de Toulouse, Toulouse.

Chowhan, Z.T., 1980. Role of binders in moisture-induced hardness increase in compressed tablets and its effect on in vitro disintegration and dissolution. J. Pharm. Sci. 69, 1–4.

Crowl, V.T., Malati, M.A., 1966. Adsorption of polymers and the stability of pigment dispersions. Discuss. Faraday Soc. 42, 301–312.

Enézian, G.M., 1972. La compression directe des comprimés à láide de la cellulose microcrystalline. Pharm. Acta Helv. 47, 321–363.

Español, P., Serrano, M., Zuniga, I., 1997. Coarse-graining of a fluid and its relation to dissipative particle dynamics and smoothed particle dynamics. Int. J. Mod. Phys. C 8, 899–908.

Fahs, A., Brogly, M., Bistac, S., Schmitt, M., 2010. Hydroxypropyl methylcellulose (HPMC) formulated films: relevance to adhesion and friction surface properties. Carbohydr. Polym. 80, 105–114.

Gama Goicochea, A., 2007. Adsorption and disjoining pressure isotherms of confined polymers using dissipative particle dynamics. Langmuir 23, 11656–11663.

Glicksman, M.E., 2000. Diffusion in Solids. Field Theory, Solid-State Principles, and Applications. Wiley-Interscience, Canada.

Gregory J., 1978. Effects of polymers on colloid stability. The Scientific Basis of Flocculation, vol. 27.

Groot, R.D., Rabone, K.L., 2001. Mesoscopic simulation of cell membrane damage, morphology change and rupture by nonionic surfactants. Biophys. J. 81, 725–736.

Groot, R.D., Warren, P.B., 1997. Dissipative particle dynamics: bridging the gap between atomistic and mesoscopic simulation. J. Chem. Phys. 107, 4423–4435.

Groot, R.D., 2003. Electrostatic interactions in dissipative particle dynamics—simulation of polyelectrolytes and anionic surfactants. J. Chem. Phys. 118, 11265–11277.

Guskova, O.A., Pal, S., Seidel, C., 2009. Organization of nanoparticles at the polymer brush-solvent interface. Europhys. Lett. 88 (3), 38006.

Hagenmaier, R., Shaw, P.E., 1990. Moisture permeability of edible films made with fatty acid and (hydroxy propyl) methylcellulose. J. Agric. Food Chem. 38, 1799–1803.

Hildebrand, J.H., 1950. The Solubility of Nonelectrolytes, 3rd ed. Reinhold Pub. Corp., New York, pp. 488.

Hoogerbrugge, P.J., Koelman, J.M.V.A., 1992. Simulating microscopic hydrodynamic phenomena with dissipative particle dynamics. Europhys. Lett. 30 (4), 191–196.

HSPiP V.3.1 Software, 2010. ⟨http://www.hansen-solubility.com/HSPiP.html⟩.

Iranloye, T.A., Parrott, E.L., 1978. Effects of compression force, particle size, and lubricants on dissolution rate. J. Pharm. Sci. 67, 535–539.

Jarray, A., Gerbaud, V., Hemati, M., 2015. Prediction of solid-binder affinity in dry and aqueous systems: work of adhesion approach vs. ideal tensile strength approach. Powder Technol. 271, 61–75.

Jiménez, A., Fabra, M.J., Talens, P., Chiralt, A., 2010. Effect of lipid self-association on the microstructure and physical properties of hydroxypropyl-methylcellulose edible films containing fatty acids. Carbohydr. Polym. 82, 585–593.

Koelmans, H., Overbeek, J.Th.C., 1954. Discuss. Faraday Soc. 18, 52–63.

Laboulfie, F., 2013. Depôt en Couche Mince d'un Multi-materiau à la Surface de Particules Solides: Application à l'enrobage de Particules Alimentaires. INPT, Toulouse.
Langevin, P., 1908. On the theory of Brownian motion. C. R. Acad. Sci. 146, 530–533 (Paris).
Lara-Hernández, B., Hernández-León, A., Villafuerte-Robles, L., 2009. Effect of stearic acid on the properties of metronidazole/methocel K4M floating matrices. Braz. J. Pharm. Sci. 45 (3), 497–505.
Liu, M., Meakin, P., Huang, H., 2007. Dissipative particle dynamics simulation of pore-scale multiphase fluid flow. Water Resour. Res. 43 (4), W04411.
Mahato, R.I., Narang, A.S., 2011. Pharmaceutical Dosage Forms and Drug Delivery, 2nd Ed. CRC Press, New York.
Mayoral, E., Nahmad-Achar, E., 2012. Study of interfacial tension between an organic solvent and aqueous electrolyte solutions using electrostatic dissipative particle dynamics simulations. J. Chem. Phys. 137, 194701.
Milani, J., Maleki, G., 2012. Hydrocolloids in food industry. In: Valdez, B. (Ed.), Food Industrial Processes—Methods and Equipment.
Mitrevej, K.T., Augsburger, L.L., 1982. Adhesion of tablets in a rotary tablet press II: effects of blending time, running time, and lubricant concentration. Drug Dev. Ind. Pharm. 8, 237–282.
Moor, H.,Riehle, U. Snap-freezing under high pressure: a new fixation technique for freeze-etching. Proceedings of the 4th European Regional Conference on Electron Microscopy, 2 (1968), 33–34.
Napper, D.H., 1983. Polymeric Stabilization of Colloidal Dispersions. Academic Press, London.
Novik, K.E., Coveney, P.V., 1997. Using dissipative particle dynamics to model binary immiscible fluids. Int. J. Modern Phys. C 8 (4), 909–918.
Novik, K.E., Coveney, P.V., 1998. Finite-difference methods for simulation models incorporating nonconservative forces. J. Chem. Phys. 109 (18), 7667–7677.
Rekvig, L., Hafskjold, B., Smit, B., 2004. Molecular simulations of surface forces and film rupture in oil/water/surfactant systems. Langmuir 20 (26), 11583–11593.
Rowe, R.C., 1977. The adhesion of film coatings to tablet surfaces—the effect of some direct compression excipients and lubricants. J. Pharm. Pharmacol. 29, 723–726.
Rowe, R.C., Sheskey, P.J., Quinn, M.E., 2009. Handbook of Pharmaceutical Excipients, 6th ed. Pharmaceutical Press, London.
Salman, A.D., Hounslow, M.J., Seville, J.P.K., 2007. Handbook of Powder Technology, Granulation, 11. Elesevier, Amsterdam.
Schlijper, A.G., Hoogerbrugge, P.J., Manke, C.W., 1995. Computer simulations of dilute polymer solutions with the dissipative particle dynamics method. J. Rheol. 39 (3), 567–579.
Schulz, S.G., Frieske, U., Kuhn, H., Schmid, G., Müller, F., Mund, C., Venzmer, J., 2005. The self-assembly of an amphiphilic block copolymer: a dissipative particle dynamics study. Tenside Surfactants Deterg. 42 (3), 180–183.
Schulz, S.G., Kuhn, H., Schmid, G., Mund, C., Venzmer, J., 2004. Phase behavior of amphiphilic polymers: a dissipative particles dynamics study. Colloid Polymer Sci. 283 (3), 284–290.
Sun, H., 1998. COMPASS: an ab initio force-field optimized for condensed-phase applications overview with details on alkane and benzene compounds. J. Phys. Chem. B 102, 7338–7364.
Tomasini, M.D., Tomassone, M.S., 2012. Dissipative particle dynamics simulation of poly(ethylene oxide)-pol(ethylethylene) block copolymer properties for enhancement of cell membrane rupture under stress. Chem. Eng. Sci. 71, 400–408.
Trofimov, S., 2003. Thermodynamic consistency in dissipative particle dynamics. Tech. Univ. Eindh., Eindhoven (Ph.D. thesis).
Venturoli, M., Smit, B., 1999. Simulating the self-assembly of model membranes. PhysChemComm 2 (10), 45–49.
Vincent, B., 1974. The effect of adsorbed polymers on dispersion stability. Adv. Colloid Interface Sci. 4, 193–277.
Walbridge, D.-J., Waters, J.A., 1966. Rheology of sterically stabilized dispersions of polymethyl methacrylate) in aliphatic hydrocarbons. Discuss. Faraday Soc. 42, 294–300.
Yalkowsky, S.H., He, Y., 2003. Handbook of Solubility Data. CRC Press, Boca Raton, FL.